Available online at www.sciencedirect.com

jmr&t
Journal of Materials Research and Technology

journal homepage: www.elsevier.com/locate/jmrt

Original Article

Chemical attack and corrosion resistance of concrete prepared with electrolyzed water

Sumit Chakraborty [a,b,*], *Romio Mandal* [a], *Subrata Chakraborty* [a], *Maurizio Guadagnini* [b], *Kypros Pilakoutas* [b]

[a] *Department of Civil Engineering, IIEST, Shibpur, Howrah 711103, India*
[b] *Department of Civil and Structural Engineering, University of Sheffield, Sheffield, S1 3JD, UK*

ARTICLE INFO

Article history:
Received 10 September 2020
Accepted 25 January 2021
Available online 3 February 2021

Keywords:
Electrolyzed water
Concrete
Durability
Sulfate and chloride attack
Corrosion

ABSTRACT

This work investigates the sulfate and chloride resistance of cement composites (mortar and concrete) manufactured using electrolyzed water. Control and electrolyzed water-based cement composites were prepared using distilled water and 30 min electrolyzed water, respectively. These were exposed to 5% Na_2SO_4, 3.5% NaCl, and a combined mixture of 5% Na_2SO_4 and 3.5% NaCl solution for 200 days. Additionally, rebar reinforced control and electrolyzed water-based samples were exposed to ambient air and 5% NaCl solution for 180 days, and their corrosion potential was monitored. For control specimens, the results show compressive strength losses of 5, 12.4, and 6.1% when exposed to the above solutions, respectively, whilst for electrolyzed water-based specimens, the losses were reduced to 1, 10.1, and 3.4%, respectively. Statistical analysis of the potential values from the accelerated corrosion tests also show reduced corrosion (58 mV less negative potential) in rebar embedded in electrolyzed water-based specimen (−548 mV at 180 days) than in control specimen (−606 mV). Based on the spectral and microstructural analysis, the enhanced durability performance of electrolyzed water-based specimens is attributed to the lower ingress of deleterious agents through the less porous and compact microstructure of the hardened composites.

© 2021 Published by Elsevier B.V. This is an open access article under the CC BY-NC-ND license (http://creativecommons.org/licenses/by-nc-nd/4.0/).

1. Introduction

The global construction industry is expected to make significant changes to address the global grand challenges of climate change, urbanization, and sustainability. Hence, modern civil infrastructure requires new materials with improved performance and sustainability. Improved performance is expected not only at early age but also in the long-term. This is because in general it is the long-term durability performance that dictates the feasibility and acceptability of new technologies [1–5], as low durability can lead to the deterioration of concrete and increase the risk of loss of use and maintenance costs [4].

Durability of concrete is governed by microstructural degradation and ingress of deleterious agents. Deterioration is

* Corresponding author.
E-mail addresses: chakrabortysumitiitkgp@gmail.com, sumit.chakraborty@sheffield.ac.uk (S. Chakraborty).
https://doi.org/10.1016/j.jmrt.2021.01.101
2238-7854/© 2021 Published by Elsevier B.V. This is an open access article under the CC BY-NC-ND license (http://creativecommons.org/licenses/by-nc-nd/4.0/).

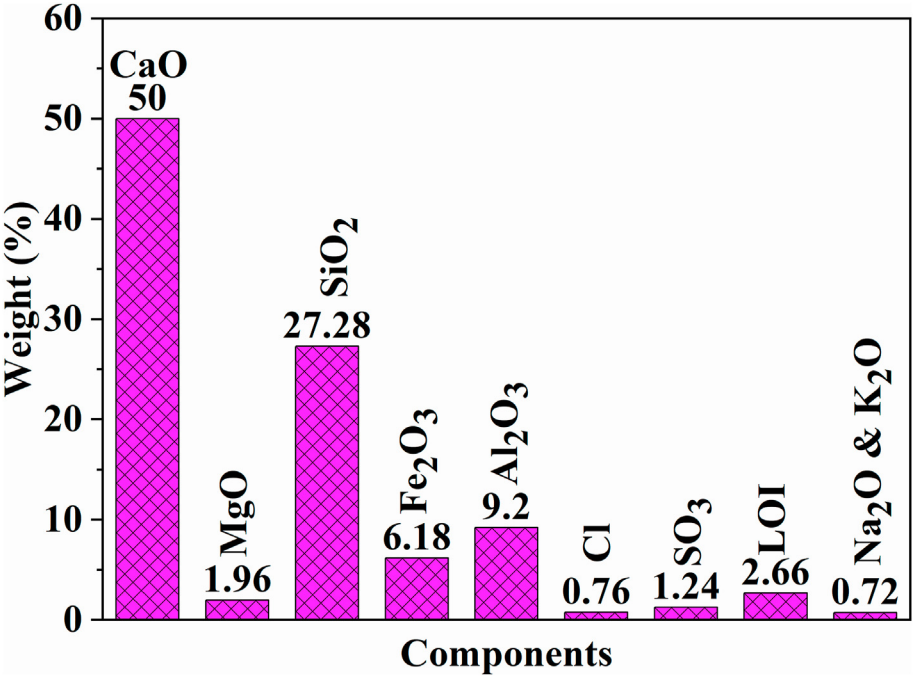

Fig. 1 – Oxide composition (in percentage) of Portland pozzolanic cement used in this study.

more frequently seen due to attack from chlorides, sulfates, and marine salt, and their combined effects [6–9], resulting in loss of both the physical and mechanical properties of concrete [1–4,10–13]. A range of chemical and mineral admixtures or alkali-activated geopolymers can be used to control the durability of concrete [14–22].

Chloride attack takes place by chloride ion permeation into the mortar/concrete from both external and internal chloride sources, which are present in the cement, aggregates, water or admixtures. Severe deterioration occurs if chloride content exceeds certain permissible limits [15]. In reinforced concrete, chloride ingress mainly causes rebar corrosion by depleting the passive layer, consisting of either α β γFeOOH or γFe_2O_3, which is self-generated on the surface of the rebar soon after the cement hydration reaction starts [23,24]. Corrosion in reinforced concrete is an electrochemical process that occurs due to the difference in electrochemical potential on the steel surface in the presence of water and oxygen [9]. This process is driven by developing anodic and cathodic regions locally connected by an electrolyte, i.e., the pore water of hardened cement [9]. Corrosion of steel produces oxides (rust), which occupy a larger volume than that of the un-corroded steel. This volume expansion leads to internal stresses that cause cracking and spalling of concrete [9,20], thus accelerating the deterioration process. To mitigate rebar corrosion, many corrosion inhibitors are available commercially [19]. Some of them aim to maintain the alkalinity of the concrete by increasing the pH of the pore solution and developing an enhanced passive layer on the rebar [23,25].

Combined sulfate and chloride attack is also responsible for the degradation of concrete structures in marine environments [9,26–28]. Sulfate ions, on their own, deteriorate concrete due to volume expansion caused by secondary ettringite and gypsum formation [9,29,30]. However, for the combined sulfate and chloride attack, the volume expansion of secondary ettringite and gypsum gets suppressed due to either less availability of C_3A and Ca^{2+}, as they react with Cl^- ions quickly to form chloroaluminate compounds and soluble calcium chloride, for the reaction with sulfate ions, or increase in solubility of gypsum and ettringite due to the reduction of pH in the presence of Cl^- ions [9,31]. However, deterioration can still occur due to the formation of pores following leaching of Ca^{2+} from the internal structural arrangement of the hydrate cement phases by dissolving the calcium-based salts, e.g., gypsum, ettringite, and calcium chloride, in the low pH solution that develops due to the ingress of Cl^- ions [8,31]. To mitigate concrete degradation in combined sulfate and chloride environments, several techniques are adopted, such as use of silica fume (SF), fly ash (FA), ground granulated blast furnace slag (GGBFS), limestone cement, and self-consolidating Portland limestone cement-based concretes [14,29,32–35].

The reported techniques and admixtures for the mitigation of the various types of chemical attack are available mainly for conventional concrete mixes. However, the durability performance of concrete formulated using cement set accelerating admixtures is yet to be investigated adequately, in particular when electrolyzed water is used as a potential set accelerating admixture [36]. Recently, the effect of electrolyzed water on setting, hydration, and physico-mechanical properties of cement composites was evaluated and reported [36–38]. It was found that electrolyzed water accelerates the setting and hydration of cement. As electrolyzed water contains a higher amount of hydroxyl ions than normal distilled water, the durability performance of the concrete mixes made with electrolyzed water is expected to be better due to lower ingress of aggressive ions through the denser microstructure (developed due to the higher rate of hydration) and thicker passive

Table 1 – Mix design of control cement composite and 30 min electrolyzed water based cement composite.

Sample Code	Type of composite	Cement (kg/m^3)	F.A.[a] (kg/m^3)	C.A.[b] (kg/m^3)	Water (kg/m^3)	Type of water used
CC	Concrete	348	709	1142	191.6	Normal distilled
30MEC	Concrete	348	709	1142	191.6	30 min electrolyzed
CC(M)	Mortar	568	1704	–	278	Normal distilled
30MEC(M)	Mortar	568	1704	–	278	30 min electrolyzed

[a] Fine aggregate.
[b] Coarse aggregate.

layer on the rebar surface. Nonetheless, it is important to establish the mechanism that drives chemical attack and rebar corrosion in electrolyzed water based concrete, so as to find ways to control them. Thus, this study investigates the durability of electrolyzed water based concrete to sulfate, chloride and combined sulfate-chloride attack, as well as resistance to normal and accelerated corrosion conditions.

2. Experimental study

Cement composite (mortar and concrete) mixes were manufactured using distilled and electrolyzed water (30 min) to produce specimens with and without embedded steel rebars, which were subsequently exposed to a range of deleterious environments to investigate their durability properties. Concrete samples prepared using distilled water and electrolyze water were designated as CC and 30MEC, respectively, whilst mortar samples were designated as CC(M) and 30MEC(M), respectively.

2.1. Raw materials

The electrolysis of water was performed using a commercially available water electrolysis device, i.e., Hydrogen Water Bottle (VYOM™, Ward Wizard Solutions Pvt. Ltd., Gujarat, India). Electrolysed water was produced by applying DC voltage between titanium and platinum electrodes separated using a semi-permeable membrane at ambient conditions (25 ± 2 °C and 65% Relative Humidity (RH)) for 30 min. The power consumption for the electrolysis device was 5 W-h, leading to small temperature increase of 4 ± 2 °C during electrolysis. After electrolysis, the hydrogen (H_2) concentration and pH of water were determined using an H_2 Sensor (Model No.: ENH-1000, TRUSTLEX, Japan) and a pH-meter (PH-08 Hydrotester, HM Digital Inc., Culver City, CA), respectively. These were found to be 0.5 ± 0.02 ppm and 9.3 ± 0.1, respectively. As the electrolyzed water shows high pH, it is anticipated that the electrolyzed water contains hydroxyl ions, see Eq. (1), which is expected to influence the hydration of cement and durability of the cement composites.

$$H_2O \xrightarrow{\text{Electrolysis}} H_2 + OH^- \text{Spontaneous} \quad (1)$$

Portland Pozzolanic Cement (PPC) conforming to IS: 1489 (part 1) [39] purchased from Ambuja Cement Ltd. was used to prepare all samples. The oxide composition of cement was assessed by wavelength dispersive X-ray fluorescence spectroscopy and is presented in Fig. 1. As expected, over 75% of the oxides are calcium and silicate. The specific gravity of cement was measured to be 2.79 [37,38] using a Le Chatelier's flask and moisture-free Kerosine of specific gravity 0.79.

Fine aggregate (FA) collected from the local market (Kolkata, India) was used to make concrete. From the sieve analysis performed in accordance with IS: 383 [40], the average particle size of FA was found to be 0.3 mm, its grading zone was II, and its specific gravity according to IS: 2386 (part 3) [41] was 2.66. Local coarse aggregate (CA) with specific gravity 2.74 measured in accordance with IS: 2386 [41], was used. Sieve analysis (in accordance with IS: 383 [40]) showed that the maximum size of CA was 20 mm.

2.2. Cement composite specimen preparation and characterization

Table 1 shows the mix ratios of the examined cement composites. The mixes were designed to achieve a strength equivalent to that of an M20 concrete in accordance with IS 10262 [42] and IS 456 [43], using a water-cement ratio (W/C) of 0.55. The mortar mixes were prepared using a ratio of cement to FA of 1:3 and W/C 0.49.

2.2.1. Preparation of concrete and mortar samples

For each mix, the dry components were mixed together before the water was added. The concrete mixes were poured into 100 mm of edge cubic moulds and vibrated using a poker vibrator. The mortar samples were cast into 70.6 mm of edge cubic moulds and vibrated using a table vibrator. For the corrosion tests, the concrete mixtures were poured into cylindrical moulds, 100 mm diameter and 200 mm height, containing a centrally place steel rebar and were vibrated using a table vibrator.

All samples were then left undisturbed for 24 h to set. After setting, the samples were removed from the moulds and allowed to cure in water for 28 days.

2.2.2. Chemical exposure

Concrete cube samples cured in water for 28 days were exposed to a combined mixture of sulfate and chloride solution (5% Na_2SO_4 and 3.5% NaCl) [29] for 200 days at ambient atmospheric conditions (25 ± 2 °C, 65% relative humidity and atmospheric CO_2 content: 408.5 ppm). Separately, mortar samples were exposed to 5% Na_2SO_4 and 3.5% NaCl solution for 200 days at ambient atmospheric conditions. Additionally, the cylindrical samples were exposed to a 5% NaCl solution at the ambient atmospheric conditions. Similar experiments were carried out by Jo et al. [23] to evaluate accelerated corrosion of reinforced concrete.

2.2.3. Mass loss and compressive strength measurements

The mass and compressive strength of three samples per mix were determined at 50 day intervals. The compressive strength was determined in accordance with IS: 516 [44], using a hydraulic universal testing machine (AIM: 31402, AMIL Ltd., India) of 2000 kN capacity at a loading rate of 13 kN min^{-1}. The mass of the samples was determined after removing them from the exposure medium and surface drying at ambient conditions for 6 h. The mass variation was calculated using Eq. (2). The mass of the concrete sample was measured using a commercial balance of 10 kg capacity showing three decimal points.

$$Mass\ gain\ (\%) = \frac{(M_{iD} - M_{28D})}{M_{28D}} \times 10 \quad (2)$$

where M_{iD} = mass of ith days exposed sample in the chemical solution and M_{28d} = mass of 28 days' water cured sample. Figs. S1a and b, see supplementary information, show the concrete cube samples exposed to the combined solution and the compressive strength testing procedure, respectively.

2.2.4. Corrosion tests

The corrosion of the embedded rebar was determined at 60 days intervals (up to 180 days) by measuring the corrosion potential at ambient conditions, using the half-cell electrode potential measurement technique in accordance with ASTM C876 [45]. Figs. S2a and b, see supplementary information, show the concrete cylinder samples exposed to 5% NaCl solution at the ambient condition (25 ± 2 °C, 65% relative humidity and 408.5 ppm atmospheric CO_2 content) and the corrosion potential measurement procedure, respectively. The corrosion potential was measured at 10 different positions to evaluate statistically the level of corrosion. The Weibull distribution was used to determine the level of corrosion at the 95% confidence level (i.e., analysis of corrosion potential values for a particular sample at 95% survival probability).

2.2.5. Weibull analysis of corrosion potential data

The Weibull distribution is a two-parameter semi-empirical distribution probability function [46–48] defined as:

$$f(x) = mx^{m-1}exp(-x^m) \quad (3)$$

where, f(x) is the frequency distribution of random variable x, and m is a shape factor generally known as Weibull modulus [46,47]. Eq. (3) is represented by a bell-shaped curve, the width of which defines the distribution of the data through *m*.

For corrosion potential, the random variable x can be defined by σ/σ_0, where σ is the corrosion potential data value and σ_0 is the normalizing parameter, i.e., corrosion potential at the (1/e) 37% survival probability. The survival probability (S) can be calculated by substituting x in equation (3) by σ/σ_0 and integrating both sides of the equation, such as:

$$S = \int_{\frac{\sigma}{\sigma_0}}^{\infty} f\left(\frac{\sigma}{\sigma_0}\right) \times d\left(\frac{\sigma}{\sigma_0}\right) = \int_{\frac{\sigma}{\sigma_0}}^{\infty} m\left(\frac{\sigma}{\sigma_0}\right)^{m-1} exp^{-\left(\frac{\sigma}{\sigma_0}\right)^m} d\left(\frac{\sigma}{\sigma_0}\right) = \exp\left[-\left(\frac{\sigma}{\sigma_0}\right)^m\right] \quad (4)$$

Inverting Eq. (4) as $1/S = \exp(\sigma/\sigma_0)^m$ and taking the logarithm on both sides of the equation twice, the final equation can be written as

$$-lnln\left(\frac{1}{S}\right) = mln(\sigma_0) - mln(\sigma) \quad (5)$$

From the plot of -lnln (1/S) versus ln(σ), a straight line with slope -*m* can be obtained. For a particular set of corrosion potential data, the σ_0 value can be calculated from the intercept and *m* from the gradient of the straight line. Hence, the physical significance of σ_0 is the value of the corrosion potential of a particular specimen/set of data at the survival probability equal to 1/e, i.e., 37%. For the determined corrosion potential data, the values of ln(σ) of CC and 30MEC were calculated using the corrosion potential values (σ) of each set of data (for a particular specimen). Table S1 (see supplementary information) summarizes the -lnln($1/S_j$) and ln(σ) for each set of data for all samples (CC and 30MEC). Then, the plots of ln(σ) vs −lnln($1/S_j$) of CC and 30MEC for different exposure duration were drawn, see Fig. S3 supplementary information, to evaluate the Weibull modulus (m) and corrosion potential (σ_0) at the survival probability = 1/e ≈ 37%. The R^2 of the plot of ln(σ) vs −lnln($1/S_j$) indicates the suitability of the Weibull model in calculating the corrosion potential statically and helps to judge the corrosion performance of CC and 30MEC at a particular exposure duration. Subsequently, the design value of the corrosion potential (σ_{design}) for each set of data (for each sample exposed for a particular duration) is calculated at the survival probability = 95% using m and σ_0 of that particular set of data.

2.2.6. Fourier transform infrared spectroscopy analysis

To identify the nature and extent of products formed in the samples, the Fourier transform infrared spectroscopy study in the attenuated total reflection mode (ATR-FTIR) of CC and 30MEC samples a) cured in water for 28 days, b) exposed to combined sulfate and chloride solution for 200 days and c) the cementitious layer deposited on the surface of steel rebar embedded in CC and 30MEC samples exposed to 5% NaCl solution for 180 days, was performed using a spectrometer (Dimond-ATR, FTIR-4700, JASCO, Japan). The samples were dried in an oven for 3 h at 85 °C [36,38] and 1 mg of powder sample was put onto the ATR sample holder before placing into the FTIR instrument to record the spectrum. A total of 16 scans were considered for the FTIR analysis for each sample in the wave number range 4000–400 cm^{-1}. The whole experimental work was conducted at controlled temperature (25 °C) and humidity (40%).

2.2.7. Microstructure analysis

To verify the microstructure of CC, 30MEC and the layer deposited on the surface of the rebar embedded in CC and 30MEC, the secondary electron mode of scanning electron microscopy (SEM) analysis was performed using a scanning electron microscope (HITACHI, S3800, Japan) with 15 kV accelerated voltage and 5kX magnification. Microstructural analysis was performed after using a sputtered thin gold coating on the sample to avoid charging.

3. Results and discussion

3.1. Mass variation of cement composites exposed to combined sulfate and chloride solution

Fig. 2 shows the mass variation of CC and 30MEC exposed to the combined sulfate and chloride solution versus exposure time. There is a small (less than 0.5%) increase in mass possibly due to the formation of further cement hydration products with time and or the precipitation of salts inside of the samples due to the ingress of sulfate and chloride ions from the exposure solution [32]. The mass increase of 30MEC is slightly smaller than that of CC, possibly due to lower ion permeation into its less porous and more compact microstructure. This concurs with the hypothesis that electrolyzed water speeds up cement hydration reactions and achieves more compact and mature microstructure with less porosity than that of the normal water based cement composites [36,38]. This hypothesis be further examined by the FTIR and SEM analysis.

3.2. Compressive strength variation of cement composites exposed to aggressive media

Fig. 3 shows the variation in compressive strength (MPa) and the rate of compressive strength change (MPa/day) of mortar samples CC(M) and 30MEC(M) exposed to (a) Na_2SO_4 and (b) NaCl solutions with exposure time. For sulfate exposure up to 100 days, Fig. 3a shows that the compressive strength of both CC(M) and 30MEC(M) increases by 26 and 18%, respectively. This strength enhancement is likely to be due to the permeation of sulfate ions and formation of gypsum and secondary ettringite in the matrix pores. The higher strength enhancement in CC(M) is likely to be due to the formation of larger amounts of secondary products by the percolation of a greater amount of deleterious ions through its higher porosity than that of 30MEC(M) [38]. Beyond 100 days of exposure, the compressive strength of both the mortar samples decreases,

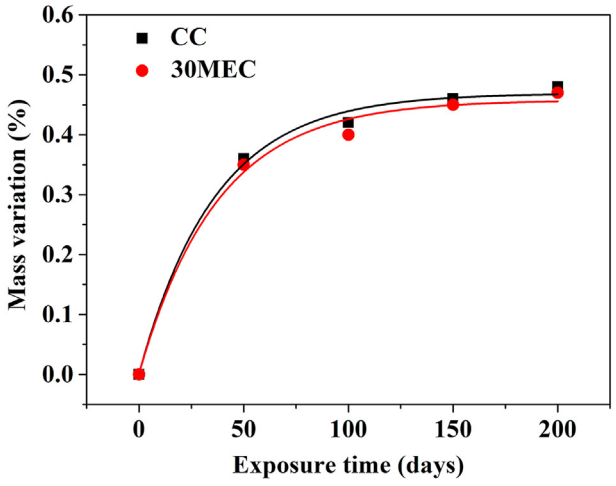

Fig. 2 – Mass variation of CC and 30MEC (concrete) specimens exposed to the combined (5% Na_2SO_4 and 3.5% NaCl) solution with increasing exposure time.

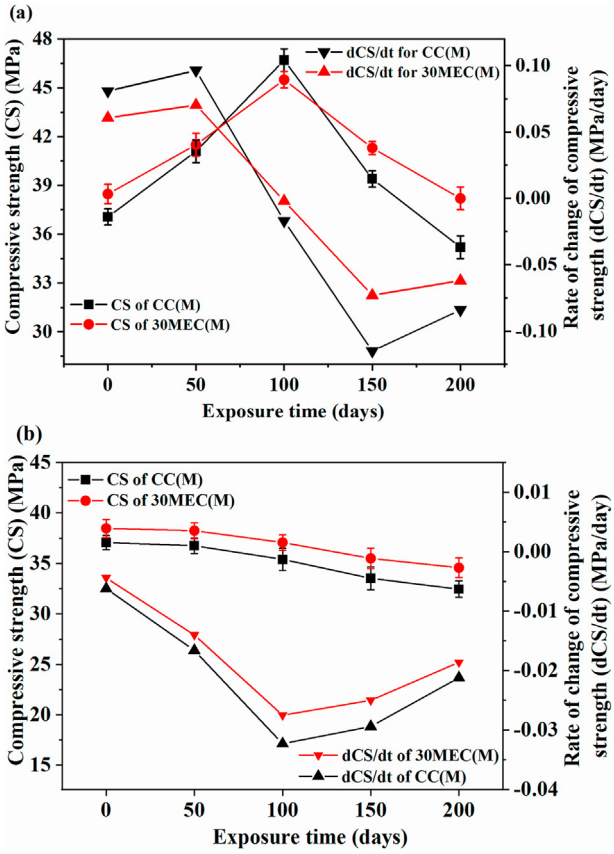

Fig. 3 – Compressive strength and rate of compressive strength versus time for mortar samples exposed to (a) 5% Na_2SO_4 solution and (b) 3.5% NaCl solution.

indicating internal degradation. This is likely to be the result of expansive pressures caused by the formation of secondary ettringite and gypsum formation [1,2]. The loss of strength is relatively lower in the 30MEC(M) samples (1% after 200 days exposure) than that of CC(M) (5%) due to its denser structure, which restricts ion penetration and secondary product formation.

For exposure to the chloride solution, it can be seen from Fig. 3b that the compressive strength of both the mortar samples decreases with exposure time. Strength losses of 12.4% and 10.1% are observed for CC(M) and 30MEC(M), respectively, after 200 days exposure. Though less severe overall degradation takes place than for sulfate exposure, the degradation starts from the beginning, with faster degradation at the early ages and slower after 100 days of exposure (see Fig. 3).

For exposure to combined sulfate and chloride solution the results are shown in Fig. 4. The compressive strength of both the concrete samples (CC and 30MEC) increases up to 150 days, followed by a slight loss at 200 days exposure. The rapid initial strength increase seen in this case may be attributed to the hydration of cement, as these samples appear to have hydrated much less than the other samples by the time they were exposed to the chemical environment. The formation of secondary products due to the permeation of sulfate and chloride ions into the concrete matrix may also have helped.

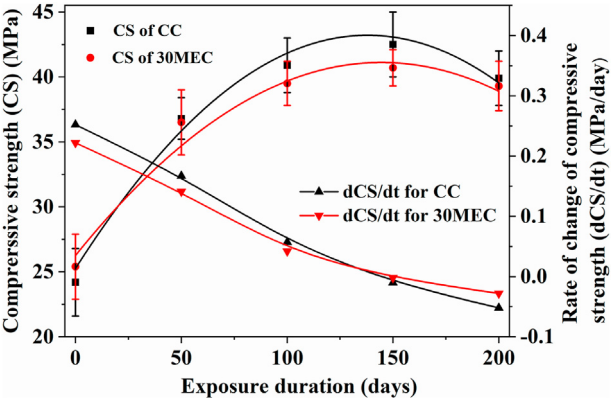

Fig. 4 – Compressive strength and rate of compressive strength versus time for CC and 30MEC (concrete) samples exposed to the combined (5% Na_2SO_4 and 3.5% NaCl) solution.

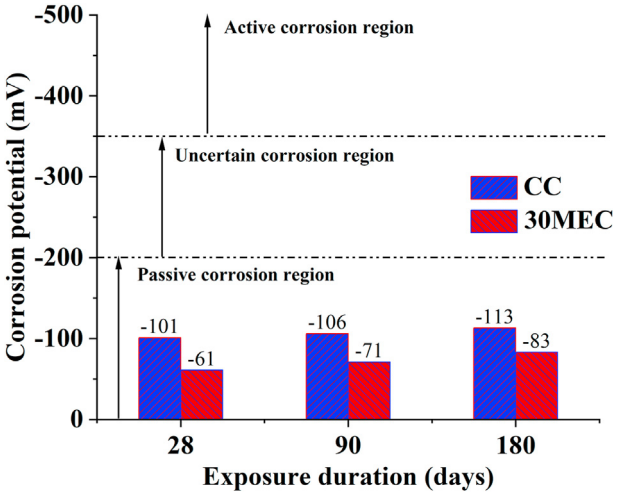

Fig. 5 – Corrosion potential value of rebar embedded in CC and 30MEC (concrete) exposed to the ambient environment (25 ± 2 °C, 65% RH, and atmospheric CO_2 content: 408.5 ppm).

The loss of strength at 200 days may be due to: (i) leaching out of Ca^{2+} ions through the formation of the soluble salts as a result of the drop in pH due to the presence of chloride ions and (ii) volume expansion due to the formation of secondary ettringite and gypsum as a result of the sulfate attack [17,25]. It appears that the sulfate attack is inhibited in the presence of the chlorides. These phenomena will be further examined by microstructural analysis.

3.3. *Corrosion analysis*

3.3.1. *Normal corrosion*

Fig. 5 shows the corrosion potential of rebar embedded CC and 30MEC samples exposed to the ambient environment up to 180 days, whilst Fig. 6 shows images of two specimens that were split open after the test. Each data point presented in Fig. 5 is the average of three data points obtained from three different positions on the circular cross-section of the specimen surface, keeping the distance between the edge of the specimen and electrode/circular line constant. The corrosion potential of both samples is less than −200 mV, indicating that no corrosion has taken place on the rebar. The analysis also reveals that the value of corrosion potential is always lower for the 30MEC samples, possibly due to the anticipated formation of a thicker passive layer on the rebar than on that embedded in CC.

3.3.2. *Accelerated corrosion*

Fig. 7 shows the corrosion potential of rebar embedded samples exposed to 5% NaCl solution versus exposure time. The corrosion potential was measured from ten different positions and the curves show the average and range. Corrosion potential values of 30MEC are consistently lower than those of CC and they enter the active corrosion stage at about 100 days of exposure, twice the time it takes for the CC specimens. This clearly shows that the use of electrolyzed water enhances the corrosion resistance of concrete. This is further verified by visual inspection, see Fig. 8a and b, of the split specimens after testing. The lower corrosion rate is likely to be due to the high pH of the electrolyzed water (9.3 ± 0.1) that facilitates the formation of a thicker passive layer around the rebar [23,25,49]. This slows down the corrosion process, but eventually the rapid chloride ion penetration into the concrete depletes the passive layer of the rebar.

3.3.2.1. *Statistical analysis of corrosion level using Weibull distribution.* The corrosion potentials measured from the 10 locations of a particular sample vary to some extent as shown in Table 2. Hence, there is a need to assess the level of corrosion for a particular sample at a particular confidence level. This was done using the Weibull distribution model considering 95% survival probability, as shown in Table 3 and Fig. 9. For each set of data, the plot of ln(σ) vs -lnln(1/Sj) shown in Fig. S3 (supplementary information) follows the linear fitting with $R^2 \geq 0.90$, demonstrating the suitability of the Weibull model to precisely predict the level of corrosion. Based on the Weibull analysis at the 95% survival probability, it is assessed that the corrosion potential of both the samples (CC and 30MEC) will not be higher (means less negative) than −585.8 and −536.2 mV, respectively, when exposed to 5% NaCl for 180 days. Additionally, it can be seen that to reach a threshold value (−350 mV) of the active corrosion potential, 30MEC takes twice the time (102 days) needed for CC (53 days). Hence, it can be anticipated that the corrosion of 30MEC is likely (95% survival probability) to be delayed by ~49 days (or ~92%) than that of CC when exposed to a 5% NaCl solution.

3.4. *Justification of observed phenomena*

The better performance of the electrolyzed water based concrete in resisting deleterious ions attack is primarily governed by the inhibition of the ion permeation through the denser microstructure developed due to the formation of a greater degree of hydrated products such as calcium-silicate-hydrate (C–S–H) and calcium hydroxide (CH). The hypothesis will be further examined by spectral (FTIR) and microstructural (SEM) analysis.

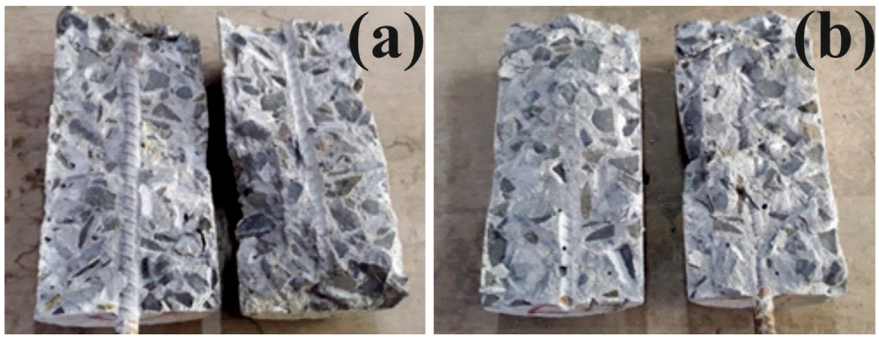

Fig. 6 – Visual inspection image of the split surface and rebar embedded in concrete exposed to ambient condition for180 days; (a) CC and (b) 30MEC.

Corrosion in reinforced concrete is an electrochemical process that occurs due to the differences in electrochemical potential on the steel surface in the presence of water and oxygen [9]. Hence, corrosion of reinforced steel occurs due to the formation of anodic and cathodic regions at tiny parts of the rebar connected by the electrolyte, i.e., pore water of hardened cement. At the anode, Fe^{2+} ions pass into the solution, whereas, electrons pass along the rebar toward cathode and combine with oxygen and water to produce hydroxyl ions [9]. These hydroxyl ions then travel through the electrolyte and combine with Fe^{2+} to form ferrous hydroxide that is subsequently converted into ferric hydroxide and then oxidized to form rust [9,20,23]. Additionally, chloride-induced corrosion occurs as chloride ions penetrate the protective oxide film (passive layer) [9] forming hydrochloric acid at the anodic side that destroys the passive layer, leaving the steel vulnerable to corrosion through the formation of rust by reacting with oxygen and moisture [9,20].

The lower corrosion of rebar embedded in electrolyzed water based concrete is likely to be due to the combination of a denser microstructure that retards the chloride penetration and the presence of a higher amount of hydroxyl ions [50] that neutralise the acid attack, slowing down the depletion of the protective oxide film (see Fig. 10).

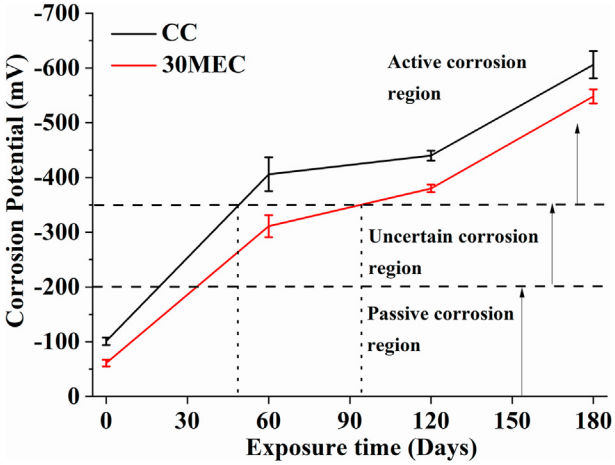

Fig. 7 – Corrosion potential value of rebar embedded in CC and 30MEC (concrete) exposed to the accelerated (5% NaCl solution) environment for 180 days (Atmospheric condition: 25 ± 2 °C, 65% RH, and atmospheric CO_2 content: 408.5 ppm).

3.4.1. *Fourier transform infrared spectroscopy (FTIR) analysis*

Fig.11 shows the FTIR spectra in transmittance mode of CC and 30MEC samples cured for 28 days in water and exposed to combined sulfate and chloride rich solution for 200 days. Additionally, the figure also represents the FTIR spectra of the cementitious layer deposited on the rebar embedded in CC and 30MEC specimen exposed to 5% NaCl solution for 180 days. The most informative bands in the IR spectrum of CC and 30MEC cured in water and exposed to combined sulfate and chloride solution appear around 1440 and 1365 cm^{-1} due to the ν_3C–O (splitting) stretching of carbonate and the band around 975 cm^{-1} that appears due to the Si–O stretching of polymeric silicate of CSH [36,51,52]. A broader IR band around 1217 cm^{-1} appears for 28 days water cured CC and 30MEC samples due to the S–O stretching of sulfate ions present in the hydrated cement [53]. However, this band is observed to be more prominent for CC and 30MEC samples exposed to the combined sulfate and chloride solution for 200 days. Moreover, it is noted that a more intense SO_4^{2-} band appears for CC than for 30MEC. This implies that a greater extent of sulfate attack takes place in CC than in 30MEC. IR band at 975 cm^{-1} of 28 days water cured 30MEC is also observed to be slightly more intense than that of CC. This clearly indicates a greater degree of hydrated product, i.e., a larger amount of Calcium-Silicate-Hydrate gel formed in 30MEC than in CC [36,38]. The formation of more hydrated products in 30MEC reduces the porosity in 30MEC as compared to that of CC [36,38], which, in turn, resists the permeation of aggressive ions. Eventually, the deterioration of 30MEC is less than that of CC when exposed to the combined solution.

IR spectra of the cementitious layer collected from the surface of the rebar of CC and 30MEC exposed to NaCl solution for 180 days show IR bands including: C–O of carbonate and Si–O of polymeric silicate, and some other bands at 877, 680, and 525 cm^{-1}. These are possibly due to the Fe–O of αFeOOH, βFeOOH, and γFe_2O_3, respectively [15,24]. These may only appear when the surface of the steel rebar oxidises by reacting with the hydrated cement products, air, and moisture [15]. IR band at 877 cm^{-1} appears to be due to the combination of ν_2 stretching of carbonate and Fe–O. Additionally, the sharp intense band around 1200 cm^{-1} is assumed to be due to the

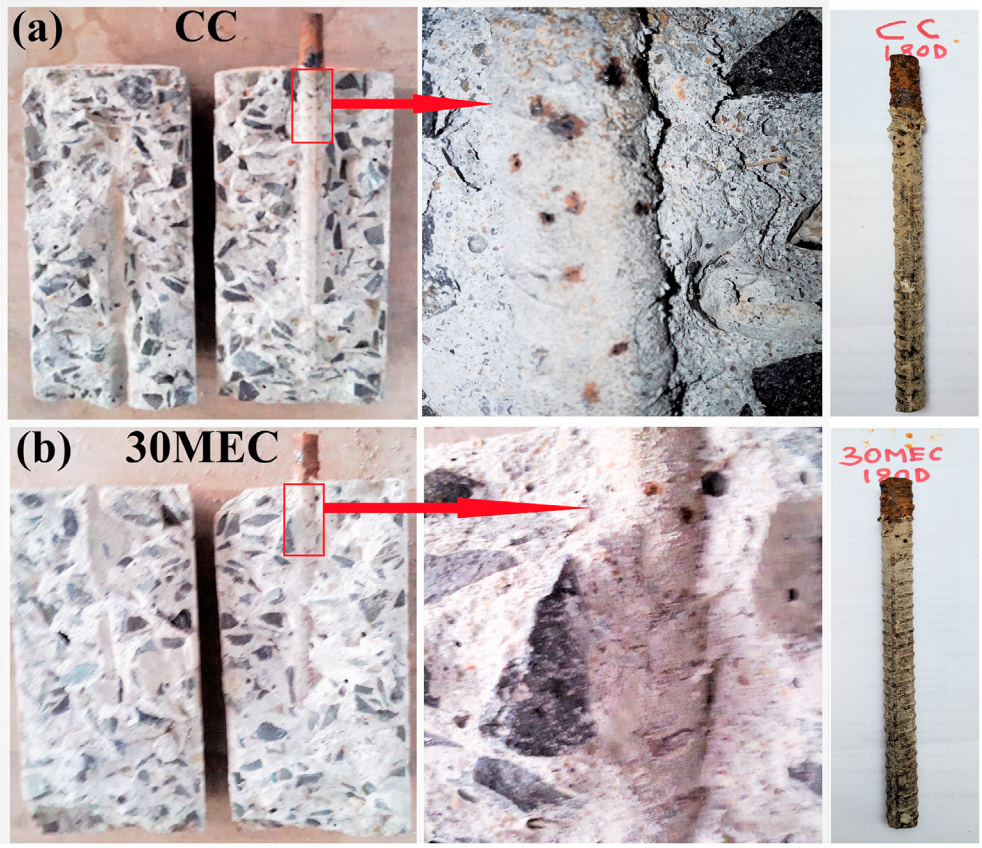

Fig. 8 – Visual inspection image of the split surface and rebar embedded in (a) CC and (b) 30MEC exposed to 5% NaCl solution for 180 days.

Si–O stretching of condensed silica [53]. In fact, the appearance of these bands in IR spectrum could be due to the combination of the passive oxide layer formed on to the steel rebar surface and the development of corrosion products. As the sample contains Fe–O bond, it can be considered to be the de-passivated (oxidised) component which was loosely bonded to the rebar surface. The collection of the strong passive layer/protective oxide film formed on to the rebar surface is more difficult because of its stability and binding ability with the rebar surface. Therefore, considering the IR bands and their intensities, it can be said that more de-passivated components (corrosion products) were formed on the rebar embedded in CC than in 30MEC as the IR band intensities of Fe–O bonds are more for the CC sample.

3.4.2. *Microstructural analysis*

Fig. 12a and b shows the SEM images of 28 days water cured CC and 30MEC, respectively. The microstructures of both the samples seem to be similarly matured. However, comparatively less flaky and compact microstructure is observed for 30MEC (Fig. 12b) than for CC (Fig. 12a), because of the formation of a greater amount of hydrated products as evidenced by the spectral analysis. A denser structure is also expected to resist more deleterious ion permeation and show less deterioration. This is investigated in Fig. 12c and d for 5% Na_2SO_4, Fig. 12e and f for 3.5% NaCl and Fig. 12g and h for the combined mixture of 5% Na_2SO_4 and 3.5% NaCl solution.

It is observed from Fig. 12c and d that both the samples CC(M) and 30MEC(M) exposed to 5% sodium sulfate solution

Table 2 – Corrosion potential measured at ten different positions of CC and 30MEC specimens exposed to 5% NaCl solution for 0, 60, 120, and 180 days (ascending order).

(j)	Corrosion potential (σ)[a] in |–mV| of CC and 30MEC exposed for different days (D)							
	CC				30MEC			
	0 D	60 D	120 D	180 D	0 D	60 D	120 D	180 D
1	90	362	421	558	54	278	368	530
2	93	372	432	573	55	290	372	533
3	95	378	435	596	56	298	375	537
4	97	386	437	599	58	303	377	542
5	99	400	440	608	60	308	379	545
6	103	415	440	617	61	313	382	548
7	103	419	445	620	64	318	383	557
8	107	427	446	624	66	325	385	561
9	108	443	449	629	69	338	388	563
10	112	456	451	634	70	340	390	565

[a] Refers to the corrosion potential of CC and 30MEC in ascending order.

Table 3 – Weibull modulus (m), σ_0 (corrosion potential at 37% survival probability), and σ_{design} (corrosion potential at 95% survival probability) of CC and 30MEC exposed to 5% NaCl solution for 0, 60, 120, and 180 days.

Weibull parameters	Values of different Weibull parameters of CC and 30MEC exposed for different days (D)							
	CC				30MEC			
	0D	60D	120D	180D	0D	60D	120D	180D
M	15.5	14	53.9	26.5	11.4	17.1	59.7	46
σ_0 (|−mV|)	103.4	424.1	443.5	620.3	93.8	380.6	431.2	554.1
σ_{design} (|−mV|)	64.5	319.3	384.3	585.8	56.5	292.2	374.7	536.2

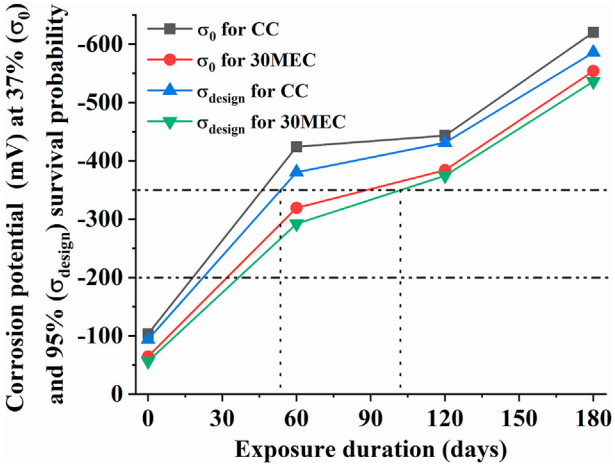

Fig. 9 – σ_0 (corrosion potential at 37% survival probability) and σ_{design} (corrosion potential at 95% survival probability) values of CC and 30MEC as the function of exposure time.

contain rod like secondary product crystals, with CC (Fig. 12c) containing more secondary gypsum crystals and flaky microstructure than 30MEC (Fig. 12d). This is likely due to the ingress of larger amounts of sulfate ions through the capillary pores of CC [38]. More gypsum crystals will lead to more volume expansion and result in faster deterioration of CC than 30MEC.

Fig. 12e and f shows the SEM images of CC(M) and 30MEC(M) samples exposed to 3.5% NaCl solution for 200 days. The microstructure of CC(M) (Fig. 12e) seems to be flaky and scattered, whilst the 30MEC(M) sample still contains some calcium hydroxide and calcium carbonate with a less scattered microstructure (Fig. 12f). The chloride ion permeation degrades the concrete matrix by destroying the stable network of hydrated products.

Gypsum seems to be formed in both CC and 30MEC samples, see Fig. 12g and h, due to the permeation of SO_4^{2-} ions [54] when they are exposed to the combined solution. As expected, more gypsum crystals are seen in CC that of 30MEC per unit area. This generation of secondary products can fill pores in CC faster and result in a better improvement in strength at the early ages of exposure. However, with prolonged exposure, further production of secondary products leads to expansive internal pressure resulting in the greater deterioration of CC than 30MEC.

Figs. 13a and b shows the SEM images of the cementitious layer deposited on the rebar embedded in CC and 30MEC exposed to 5% NaCl solution for 180 days. It appears that CC contains iron oxides (needle like structures),

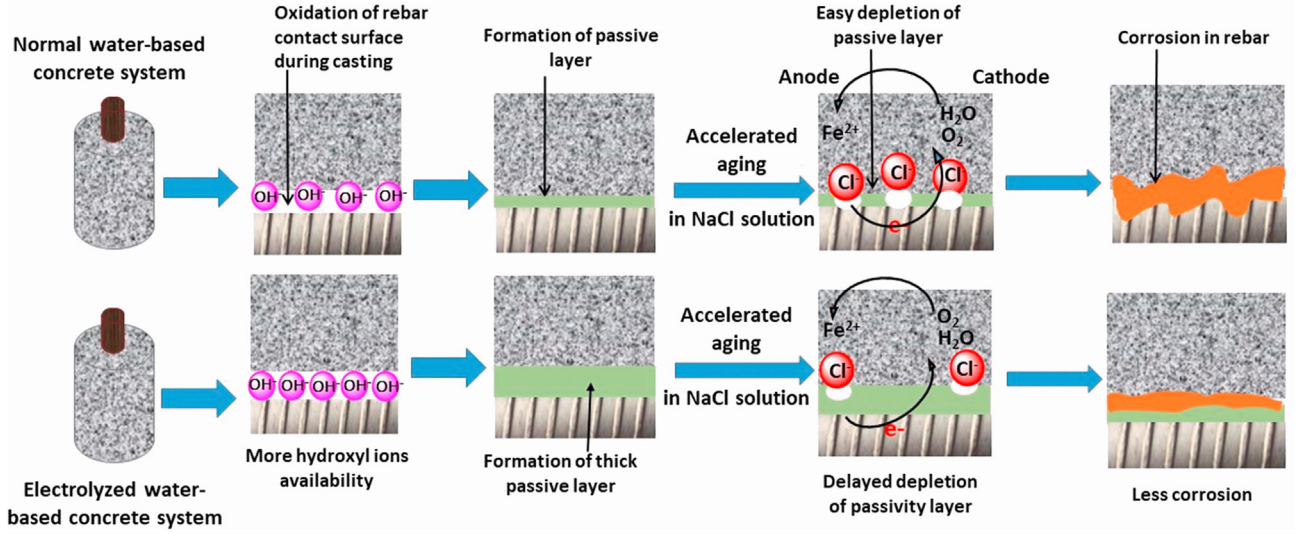

Fig. 10 – A plausible model to explain the corrosion mechanism of rebar embedded in the normal and electrolyzed water based concrete exposed to NaCl solution.

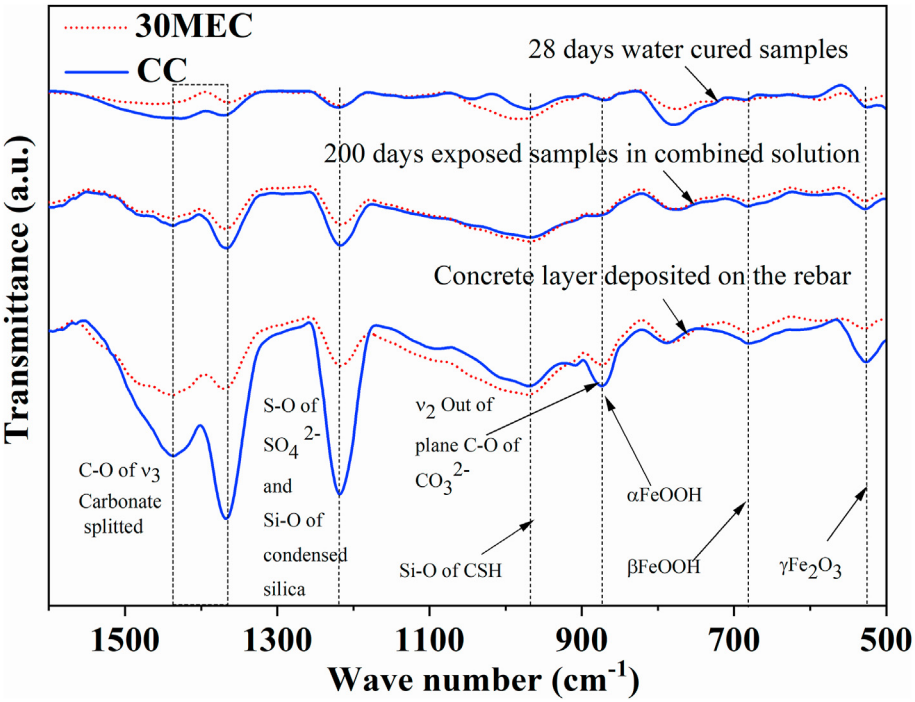

Fig. 11 – FTIR spectra of CC and 30MEC (concrete) cured in water for 28 days, exposed to the combined (5% Na_2SO_4 and 3.5% NaCl) solution for 200 days, and the layer deposited on the rebar embedded in CC and 30MEC exposed to 5% NaCl solution for 180 days. IR band description: 1440 cm^{-1} and 1365 cm^{-1}: ν_3C–O (splitting) stretching of carbonate, 975 cm^{-1}: Si–O stretching of polymeric silicate of CSH, around 1200 cm^{-1}: Si–O of condensed silica, 1217 cm^{-1}: S–O of SO_4^{2-}, 877 cm^{-1}: Fe–O of αFeOOH, 680 cm^{-1}: Fe–O of βFeOOH, and 525 cm^{-1}: Fe–O of and γFe_2O_3.

i.e., possibly goethite (αFeOOH) and akaganeite (βFeOOH) like structures [24], which may grow at the interface region of rebar surface and cementitious layer. However, no such type of crystal is observed in the microstructure of the cementitious layer collected from the rebar surface of 30MEC. The appearance of iron oxide in the cementitious layer of CC is presumed to be due to the depletion of the passive film on the rebar surface by the ingress of Cl^- ions and corrosion due to presence of moisture and oxygen. As there is no trace of iron oxide in the microstructure of the cementitious layer of 30MEC, it can be seen as evidence of the higher resilience of its passive film, which protects the rebar from the corrosion.

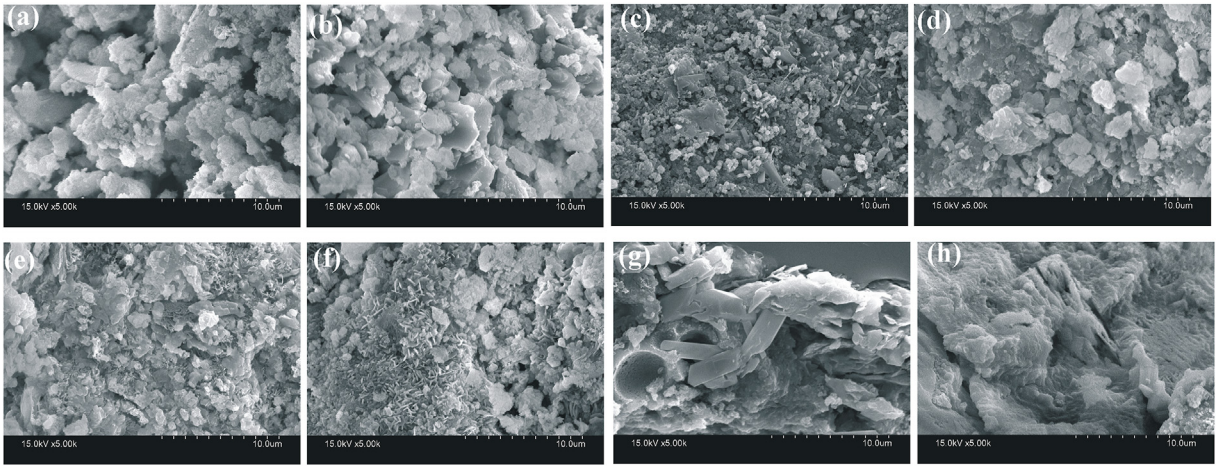

Fig. 12 – SEM image of 28 days water cured (a) CC and (b) 30MEC, 200 days exposed to Na_2SO_4 solution (c) CC(M) and (d) 30MEC(M), 200 days exposed to NaCl solution (e) CC(M) and (f) 30MEC(M), and 200 days exposed to the combined sulfate and chloride rich (5% Na_2SO_4 and 3.5% NaCl) solution (g) CC and (h) 30MEC.

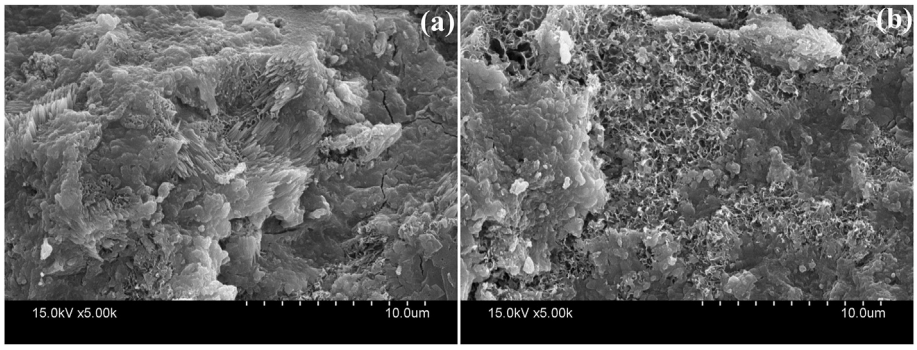

Fig. 13 – SEM image of the cementitious layer deposited on the rebar embedded in (a) CC and (b) 30MEC exposed to 5% NaCl solution for 180 days.

4. Conclusions

This study provides new insight into the long term performance of concrete and mortar made with electrolyzed water by evaluating the chemical attack and the level of rebar corrosion resistance under both normal and accelerated conditions. The impact of electrolyzed water in controlling the durability performance of concrete was assessed by exposing the mortar and concrete samples to sulfate (5% Na_2SO_4), chloride (3.5% NaCl) and combined sulfate and chloride solution. For these samples mass and strength variation was monitored with time. Additionally, rebar embedded samples exposed to ambient environment and 5% NaCl solution were monitored for corrosion potential. The conclusions from this study were:

- When exposed to sulfates, an increase in the compressive strength of both samples was observed up to 100 days due to the densification of the pore structures through the formation of secondary gypsum products. However, further generation of secondary products eventually led to strength degradation due to expansive internal pressures.
- Gradual strength loss was seen due to chloride exposure associated with dissolution of stable hydrated cement phases.
- The combined chemical attack combined the effect of sulfate and chloride attack and led to concrete deterioration in the long term (200 days).
- Corrosion potential was developed faster in CC specimens, which showed active corrosion after ~53 days, whilst the 30MEC samples resisted until 102 days. Hence, for design purposes, it can be anticipated that the concrete made with electrolyzed water takes twice the time as much of normal water based-concrete to develop active corrosion.
- The improved durability and corrosion resistance performance of the concrete prepared using electrolyzed water (30MEC) is found to be due to the formation of a more compact microstructure, enhancement of stable passivation layer on the rebar surface, and the lesser permeation of aggressive ions.

Based on the experimental evidences obtained from this study, it can be said that electrolyzed water has enough potential to enhance chemical attack resistance and mitigate corrosion in precast and in-situ concrete infrastructure exposed to severe environments such as ground, marine and wastewater constructions.

Declaration of Competing Interest

The authors don't have any conflict of interests.

Acknowledgments

The authors would like to acknowledge the funding agency SERB, Govt. of India for their funding (Project No. YSS/2015/001393) and the European Union for funding the Marie Skłodowska-Curie Individual Fellowship under grant agreement No 838623. This project was supported by the Royal Academy of Engineering under the Research Chairs and Senior Research Fellowships scheme.

Appendix A. Supplementary data

Supplementary data to this article can be found online at https://doi.org/10.1016/j.jmrt.2021.01.101.

REFERENCES

[1] Jo BW, Sikandar MA, Chakraborty S, Baloch Z. Investigation of the acid and sulfate resistance performances of hydrogen-rich water based mortars. Construct Build Mater 2017;137:1–11.
[2] Liu PC. Damage to concrete structures in a marine environment. Mater Struct 1991;24:302–7.
[3] Zuquan J, Wei S, Yunsheng Z, Jinyang J, Jianzhong L. Interaction between sulfate and chloride solution attack of concretes with and without fly ash. Cement Concr Res 2007;37(8):1223–32.

[4] Tang SW, Yao Y, Andrade C, Li ZJ. Recent durability studies on concrete structure. Cement Concr Res 2015;78:143–54.
[5] Zhang Z, Wang Q, Chen H, Zhou Y. Influence of the initial moist curing time on the sulfate attack resistance of concretes with different binders. Construct Build Mater 2017;144:541–51.
[6] Ramezanianpour AA, RiahiDehkordi E. Effect of combined sulfate-chloride attack on concrete durability-A review. AUT J Civil Eng 2017;1(2):103–10.
[7] Shaikhon O. The effect of chloride and sulfate ions on the resistivity of concrete. Doctoral dissertation. Montréal: McGill University Libraries; 2016.
[8] ACI 515.2R-13. Guide to selecting protective treatments for concrete ACI committee 515. Farmington Hills, MI, USA: American Concrete Institute; 2013.
[9] Naville AM, Brooks JJ. Concrete technology. England: Longman Scientific & Technical; 1987.
[10] Alawi Al-Sodani KA, Maslehuddin M, AlAmoudi OSB, Saleh TA, Shameem M. Performance of corrosion inhibitors in cracked and un-cracked silica fume cement concrete beams. Euro J Environ Civil Eng 2020;24(10):1573–88.
[11] Al-Amoudi OSMB, Al-Homidy AAK, Maslehuddin M, Saleh TA. Method for enhancing strength and durability of weak soils. Patent United States: US9499742B2, 2016.
[12] Saleh TA, editor. Nanotechnology in oil and gas industries. Springer International Publishing; 2018. https://doi.org/10.1007/978-3-319-60630-9. 978-3-319-60630-9.
[13] Al-Amoudi OSB, Al-Homidy AA, Maslehuddin M, Saleh TA. Method and mechanisms of soil stabilization using electric arc furnace dust. Sci Rep 2017;7(46676):1–10.
[14] Duan P, Shui Z, Chen W, Shen C. Enhancing microstructure and durability of concrete from ground granulated blast furnace slag and metakaolin as cement replacement materials. J Mater Res Technol 2013;2(1):52–9.
[15] Neville AM. In: Properties of concrete, vol. 4. London: Longman; 1995.
[16] Ramachandran D, George RP, Vishwakarma V, Mudali UK. Strength and durability studies of fly ash concrete in sea water environments compared with normal and superplasticizer concrete. KSCE J Civil Eng 2017;21(4):1282–90.
[17] Tayeh BA, AlSaffar DM, Alyousef R. The utilization of recycled aggregate in high performance concrete: a review. J Mater Res Technol 2020;9(4):8469–81.
[18] Mailvaganam N, Rixom R. Chemical admixtures for concrete. 3rd ed. London: E&FN Spon; 1999. 11 New Fatter Lane.
[19] Abdulrahman AS, Ismail M, Hussain MS. Corrosion inhibitors for steel reinforcement in concrete: a review. Sci Res Essays 2011;6(20):4152–62.
[20] Portland Cement Association [US]. America's cement manufactures. Available at: https://www.cement.org/learn/concrete-technology. [Accessed 12 September 2020].
[21] Al-Jamimi HA, Al-Azani S, Saleh TA. Supervised machine learning techniques in the desulfurization of oil products for environmental protection: a review. Process Saf Environ Protect 2018;120:57–71.
[22] Al-Sodani KAA, Maslehuddin M, Al-Amoudi OSB, Saleh TA, Shameem M. Efficiency of generic and proprietary inhibitors in mitigating corrosion of carbon steel in chloride-sulfate environments. Sci Rep 2018;8(11443):1–13.
[23] Jo BW, Sikandar MA, Chakraborty S, Baloch Z. Investigation of corrosion assessment of hydrogen-rich water based cement mortars. J Ceram Process Res 2017;18(4):305–12.
[24] Dhaiveegan P, Elangovan N, Nishimura T, Rajendran N. Weathering steel in industrial-marine-urban environment: field study. Mater Trans 2016;57(2):148–55.
[25] Paul SC, Babafemi AJ. A review on reinforcement corrosion mechanism and measurement methods in concrete. Civil Eng Res J 2018;5(3):1–11.
[26] Maes M, Belie ND. Resistance of concrete and mortar against combined attack of chloride and sodium sulphate. Construct Build Mater 2014;53:59–72.
[27] Song HW, Pack SW, Ann KY. Probabilistic assessment to predict the time to corrosion of steel in reinforced concrete tunnel box exposed to sea water. Construct Build Mater 2009;23:3270–8.
[28] Kwon SJ, Na UJ, Park SS, Jung SH. Service life prediction of concrete wharves with early-aged crack: probabilistic approach for chloride diffusion. Struct Saf 2009;31:75–83.
[29] Jo BW, Chakraborty S, Lee ST, Lee YS. Durability study of silica fume-mortar exposed to the combined sulfate and chloride-rich solution. KSCE J of Civil Eng 2019;23(1):356–66.
[30] Divet L, Pavoine A. Delayed ettringite formation in massive concrete structures: an account of some studies of degraded bridges. Int. RILEM TC 2004:98–126.
[31] Santhanam M, Cohen M, Olek J. Differentiating seawater and groundwater sulfate attack in Portland cement mortars. Cement Concr Res 2006;36:2132–7.
[32] Li G, Zhang A, Song Z, Liu S, Zhang J. Ground granulated blast furnace slag effect on the durability of ternary cementitious system exposed to combined attack of chloride and sulfate. Construct Build Mater 2018;158:640–8.
[33] Sotiriadis K, Nikolopoulou E, Tsivilis S. Sulfate resistance of limestone cement concrete exposed to combined chloride and sulfate environment at low temperature. Cement Concr Compos 2012;4:903–10.
[34] Chiker T, Aggoun S, Houari H, Siddique R. Sodium sulfate and alternative combined sulfate/chloride action on ordinary and self-consolidating PLC-based concretes. Construct Build Mater 2016;106:342–8.
[35] Jo BW, Sikandar MA, Chakraborty S, Baloch Z. Strength and durability assessment of Portland cement mortars formulated from hydrogen-rich water. Ann Mater Sci Eng 2017;2017(2526130):1–10.
[36] Mandal R, Chakraborty S, Chakraborty P, Chakraborty S. Development of the electrolyzed water based set accelerated greener cement paste. Mater Lett 2019;243:46–9.
[37] Mandal R, Chattopadhyay S, Chakraborty S, Chakraborty P, Chakraborty S. Development of electrolyzed water based concrete: a new approach for early strength gain. In: UKIERI concrete congress; 2019. https://ukiericoncretecongress.com/Home/files/Proceedings/pdf/UCC-2019-193.pdf. [Accessed 9 July 2019].
[38] Chakraborty S, Mandal R, Chattopadhyay S, Chakraborty S. Investigation on the effectiveness of electrolyzed water in controlling the early age properties of cement mortar. Construct Build Mater 2019;211:1–11.
[39] IS: 1489 (part 1) -1991. Portland-pozzolana specification, fly ash based. New Delhi, India: BIS; 2005.
[40] IS: 383 -2016. Coarse and fine aggregate for concrete-specification. New Delhi, India: BIS; 2016.
[41] IS: 2386 (part 3) -1963. Methods of test for aggregates for concrete. New Delhi, India: BIS; 2002.
[42] IS: 10262-2009. Concrete mix proportioning – guidelines. New Delhi, India: BIS –; 2009.
[43] IS: 456-2000. Plain and reinforced concrete code of practice. New Delhi, India: BIS; 2005.
[44] IS: 516 -1959. Methods of tests for strength of concrete. New Delhi, India: BIS; 2004.
[45] ASTM C 876. Standard test method for corrosion potentials of uncoated reinforcing steel in concrete. West Conshohocken, Pennsylvania, USA: American Society for Testing and Materials; 2009.

[46] Barsoum MW. In: Fundamentals of ceramics. International Ed. India: The McGraw Hill Companies; Series in material science and engineering; 1997.
[47] Jo BW, Chakraborty S, Sikandar MA, Lee YS. Prediction of the failure stress of hydrogen-rich water based cement mortar using the Weibull distribution model. KSCE Journal of Civil Eng 2017;22:1827–39.
[48] Roy A, Chakraborty S, Kundu SP, Basak RK, Majumder SB, Adhikari B. Improvement in mechanical properties of jute fibres through mild alkali treatment as demonstrated by utilization of the Weibull distribution model. Bioresour Technol 2012;107:222–8.
[49] Yoo DY, Gim JY, Chun B. Effects of rust layer and corrosion degree on the pullout behavior of steel fibers from ultra-high-performance concrete. J Mater Res Technol 2020;9(3):3632–48. https://doi.org/10.1016/j.jmrt.2020.01.101.
[50] Jiang JY, Wang D, Chu HY, Ma H, Liu Y, Gao Y, et al. The passive film growth mechanism of new corrosion-resistant steel rebar in simulated concrete pore solution: nanometer structure and electrochemical study. Materials 2017;10(4):412.
[51] Database of ATR-FT-IR spectra of various materials. Available at: http://lisa.chem.ut.ee/IR_spectra/paint/fillers/ironiii-oxide/. [Accessed 17 July 2019].
[52] Behera PK, Moon APK, Mondal K, Misra S. Estimating critical corrosion for initiation of longitudinal cracks in RC structures considering phases and composition of corrosion products. J Mater Civ Eng 2016;28(12):04016158.
[53] Ylmen R, Jaglid U. Carbonation of Portland cement studied by diffuse reflection fourier transform infrared spectroscopy. Int J Concr Struct Mater 2013;7(2):119–25.
[54] Wang YW, Meldrum FC. Additives stabilize calcium sulfate hemihydrate (bassanite) in solution. J Mater Chem 2012;22:22055–62.